Electronic Supplementary Information

Unveiling the dynamic CO_2 capture performance of MgO promoted with molten salts and $CaCO_3$ via fixed bed reactor experiments

Theodoros Papalas[1,2], Andy N. Antzaras[1], Angeliki A. Lemonidou[1,3*]*

[1]Department of Chemical Engineering, Aristotle University of Thessaloniki,

University Campus, 54124 Thessaloniki, Greece

[2]Department of Chemical Engineering and Biotechnology, University of Cambridge,

Philippa Fawcett Drive, CB3 0AS Cambridge, United Kingdom

[3]Chemical process & Energy Resource Institute, CPERI/CERTH, 57001 Thermi,

Thessaloniki, Greece

*Corresponding authors

Angeliki A. Lemonidou, Email: alemonidou@cheng.auth.gr

Theodoros Papalas, Email: tp557@cam.ac.uk

S.1 Supplementary content of the experimental section

Evaluation of the performance of the $MgCa_{0.05}A_{0.20}$ material in the TGA experiments was based on the CO_2 capture capacity and MgO conversion attained in the carbonation stage over cycles. The former was calculated (Eq. (S1)) by dividing the weight increase recorded at the end of carbonation (WI), which corresponds to the total amount of captured CO_2, with the weight of material recorded after the pre-treatment step (W_{in}). The conversion of MgO (X_{MgO}) was defined (Eq. (S2)) as the MgO moles that reacted ($N_{MgO,react}$), divided by the MgO moles available after pre-treatment ($N_{MgO,in}$). The latter was found by accounting the MgO weight fraction in the material (X_w) and the molecular weight of MgO (M_w).

$$CO_2 \ capacity, TGA \ (\frac{mmol_{CO2}}{g_{material}}) = \frac{WI}{44 \times W_{in}} \tag{S1}$$

$$MgO \ covnersion, TGA \ (\%) = 100 \times \frac{N_{MgO,react}}{N_{MgO,in}} = 100 \times \frac{M_w \times WI}{44 \times W_{in} \times X_w} \tag{S2}$$

Figure 1 presents the bench-scale fixed bed (FB) reactor unit used to conduct the carbonate looping experiments. The flow of gas inlet components is controlled using mass flow controllers (MFC, Brooks Instruments). A pneumatic three-way valve directs the incoming flow of the mixed gases, determining whether the experiment will be conducted under dry or wet operating conditions. The one pathway leads the gas flow through a vessel containing distilled water in controlled temperature, enabling the gas flow to be saturated with steam. The partial pressure of steam of the gas outlet would be equal to the saturation pressure determined by the temperature of the vessel. The other pathway leads the gas feed directly to the entrance of the reactor, securing dry conditions. The gas flow is fed from the top of a 20 mm OD quartz reactor, in a fixed bed configuration. The reactor is equipped with a thermowell, fitting coaxial

thermocouples at various locations of the reactor to monitor the temperature of the solids, along with a fritted quartz disc to support the material bed. The reactor is positioned within an electrically heated tubular furnace with three independently controlled temperature zones. The outlet of the reactor is directed to a condenser with a circulating cooling bath to liquify condensable components before the product analysis section, composed of a single-beam nondispersive infrared (NDIR) gas analyser (ZRE, Fuji Electric) for continuous monitoring of the CO_2 concentration. All system components are interconnected using stainless steel tubing with diameters of 1/4" OD or 1/8" OD, while check valves are positioned in different places to prevent backflow. Certain lines are heated to prevent the condensation of steam.
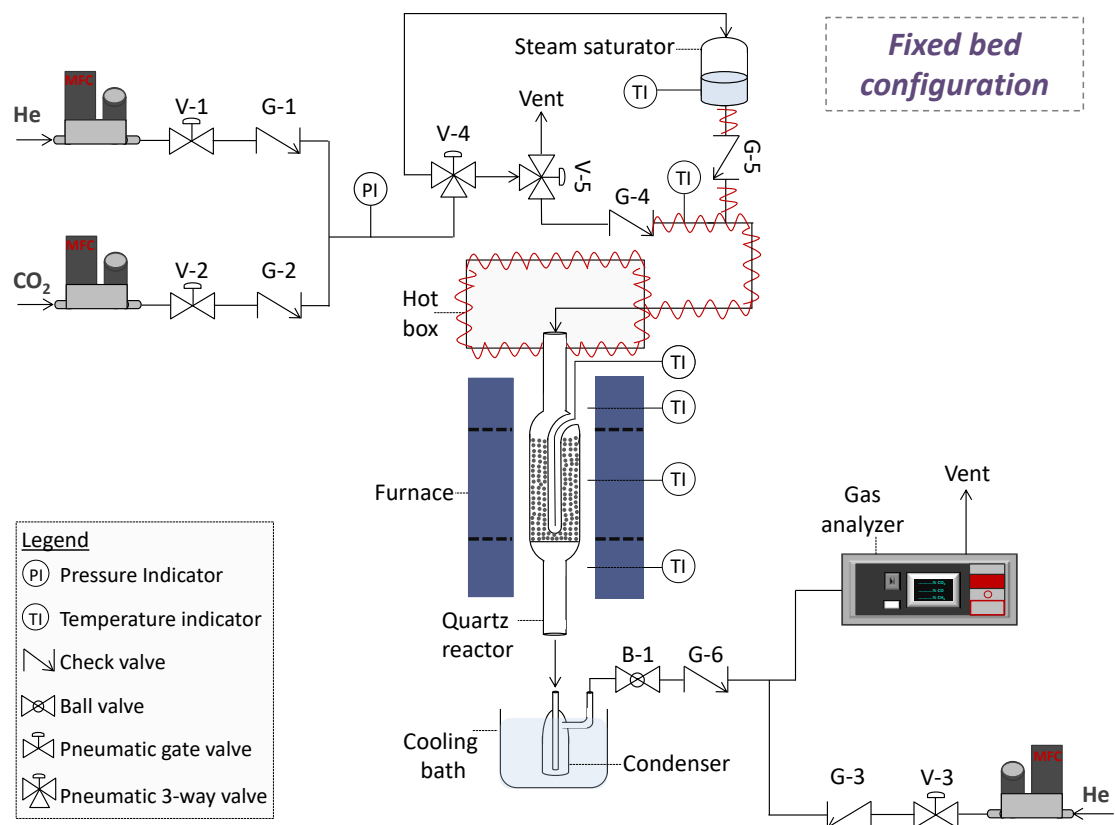
Figure S1. *Schematic layout of bench-scale unit used for carbonate looping experiments*

For the analysis of the results obtained from the carbonate looping experiments in the fixed bed reactor, the CO_2 concentration in the reactor outlet was recorded over time *via* the gas

analyser. The CO_2 capture efficiency and rate were calculated (Eqs. (S3) and (S4) respectively) by dividing the difference between the CO_2 inlet ($F_{CO2,in}$) and outlet ($F_{CO2,out}$) molar flows with the inlet molar flow or total weight of material in the bed (W_{in}) respectively. The MgO carbonation conversion was also calculated (Eq. (S5)) as the number of CO_2 moles that were captured in the total duration of the carbonation stage t_{carb}, divided by the theoretical maximum CO_2 uptake. Similarly to the equation proposed for the TGA experiments (Eq. (S2)), the theoretical uptake can be found from the total weight of material in the bed, the weight fraction (X_w) and the molecular weight (M_w) of the MgO phase. Moreover, the dynamic signal of CO_2 ($F_{CO2,out}$) enabled the calculation of the quantity released during the whole duration (t_{decarb}) of the decarbonation stage, while its comparison with the theoretical amount that can be captured enabled the calculation of the conversion of $MgCO_3$ and $CaMg(CO_3)_2$ (Eq. (S6)). Finally, the CO_2 capture capacity was found by dividing the CO_2 moles captured by the weight of material in the reactor (Eq. (S7)).

$$CO_2 \text{ } capture \text{ } efficiency \text{ } (\%) = \frac{F_{CO2,in} - F_{CO2,out}}{F_{CO2,in}} \times 100 \qquad (S3)$$

$$CO_2 \text{ } capture \text{ } rate \text{ } (\frac{mmol_{CO2}}{min \times g_{material}}) = \frac{F_{CO2,in} - F_{CO2,out}}{W_{in}} \times 100 \qquad (S4)$$

$$MgO \text{ } conversion, FB \text{ } (\%) = 100 \times M_w \times \frac{\int_0^{t_{carb}}(F_{CO2,in,blank} - F_{CO2,out})dt_{carb}}{W_{in} \times X_w} \qquad (S5)$$

$$MgCO_3/CaMg(CO_3)_2 \text{ } conversion \text{ } (\%) = 100 \times M_w \times \frac{\int_0^{t_{decarb}}(F_{CO2,out})dt_{decarb}}{W_{in} \times X_w} \qquad (S6)$$

$$CO_2 \text{ } capture \text{ } capacity, FB \text{ } (\frac{mmol_{CO2}}{g_{material}}) = \frac{\int_0^{t_{carb}}(F_{CO2,in} - F_{CO2,out})dt_{carb}}{W_{in}} \qquad (S7)$$

The validity of the results was secured by checking the carbon balance in each carbonation and decarbonation cycle. This required for the total CO_2 molar flow added during the whole duration of the carbonation stage to be equal to the sum of the total CO_2 molar flow at the reactor exit stream of the same stage and the total CO_2 molar flow at the reactor exit of the subsequent decarbonation stage (Eq. (S8)). For all experiments, the error of carbon balance was maintained below 5%. Additionally, validity was evaluated by examining the deviation between the MgO and $MgCO_3$/$CaMg(CO_3)_2$ conversions.

$$\int_0^{t_{carb}} F_{CO2,in} dt_{carb} = \int_0^{t_{carb}} F_{CO2,out} dt_{carb} + \int_0^{t_{decarb}} F_{CO2,out} dt_{decarb} \tag{S8}$$

Used materials obtained after fixed bed reactor experiments were analysed using X-Ray Diffraction (XRD). This analysis was conducted on a D8 Advance diffractometer (Bruker), employing Cu Kα radiation with a wavelength of 0.15406 nm. Diffraction patterns were recorded over a 2θ range of 20-80° with a step size of 0.02°. Moreover, the Brunauer-Emmett-Teller (BET) surface area and pore volume of the fresh material before and after pelletisation were retrieved *via* N_2 adsorption, performed at -196°C using an Autosorb-1 flow apparatus (Quantachrome Instruments). Prior to measurements, samples underwent overnight degassing under vacuum conditions at 200°C.

S.2 Supplementary content of the results and discussion section

Figure S2a illustrates the XRD patterns of fresh $MgCa_{0.05}A_{0.20}$ and used materials obtained after the final decarbonation stage of the 10-cycle experiments conducted in the FB reactor. The fresh material exhibited MgO and $CaCO_3$ as the main crystalline phases, while alkali nitrates retained their initial form as proven by the respective diffractions of KNO_3 and $NaNO_3$. Conversely, $LiNO_3$ peaks were not detected, likely due to the small crystal size of $LiNO_3$, or its existence in the amorphous phase.[1–3]
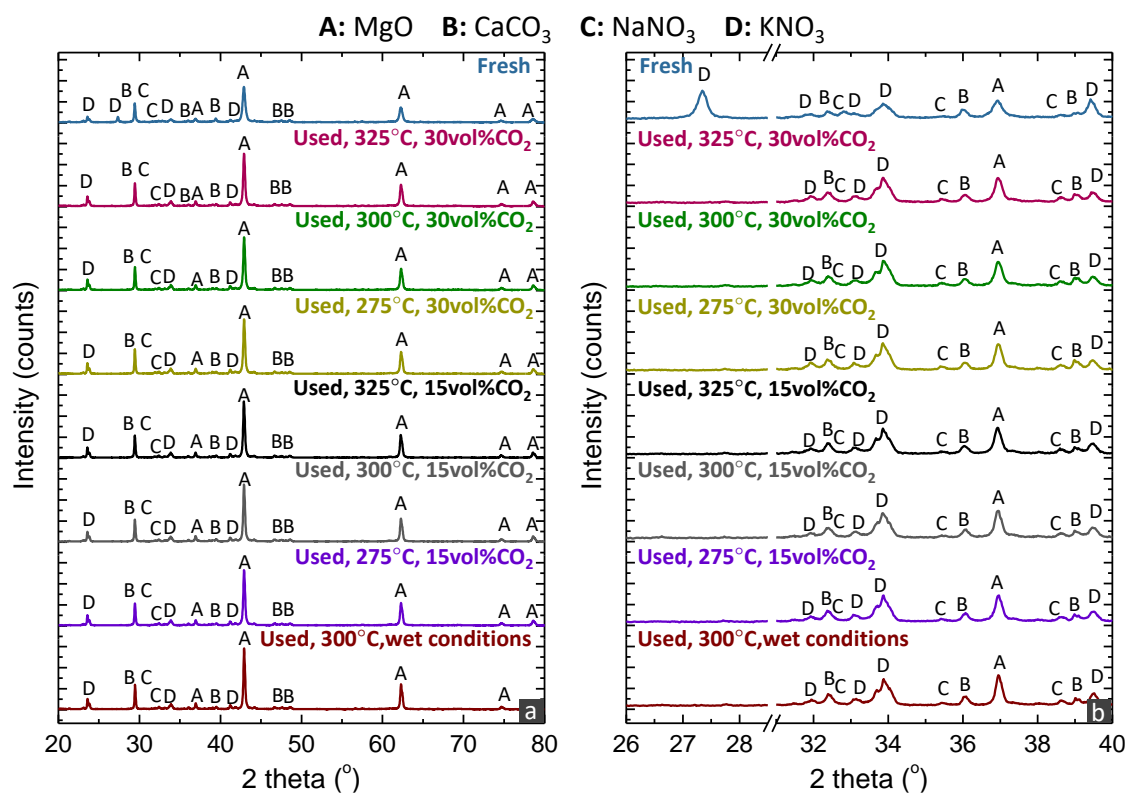
Figure S2. *XRD diffractograms for fresh and used materials after FB experiments in a 2θ range of (a) 20-80 and (b) 26-40°.*

After completion of experiments, the XRD patterns of the used materials were very similar to the original, although peaks were sligthly sharper, indicating an increase in crystallinity due to the exposure at high temperatures. The enhanced crystallinity is supported by the increase in the crystal size of MgO in used materials, as presented in **Table S1**. Despite the larger crystal size and the apparent sintering of the active phase, the material demonstrated high stability over the 10-cycle experiments. As discussed in the main paper, the high stability is a result of possible alkali salt redistribution at the surface. Notably, the greatest increase in crystal size was observed in the experiment conducted under wet conditions, due to the mineralisation effect of H_2O that promotes the extent of sintering.[4]

An additional interesting phenomenon in used materials was the slight variation of the KNO_3 peaks compared to the fresh material. The most significant example was the

absence of a KNO_3 peak at 2θ of ~27.3° (**Figure S2b**). Previous findings, including our initial findings, have indicated that KNO_3 can exist in both orthorhombic and rhombohedral structures.[1,2] The rhombohedral phase forms during the recrystallization of KNO_3 after cooling down from the calcination of the material preparation protocol. Even though some KNO_3 reverted to orthorhombic form upon cooling below ~110°C, a portion of it remained to its rhombohedral structure. Chen *et al.* witnessed that the ratio of the orthorombic to rhomohedral structure can change during the experiments, as also seen in this work, which may also be a factor affecting the stability of the material.[2]

Table S1. *MgO crystal size for fresh and used materials obtained after FB experiments.*

a/a	State	Carbonation operating conditions		Crystallite size of MgO (nm)
		Temperature (°C)	Flow composition (-)	
1	Fresh	-	-	27.5
2	Used	325	30%CO_2/He	33.2
3	Used	300	30%CO_2/He	33.8
4	Used	275	30%CO_2/He	34.0
5	Used	325	15%CO_2/He	34.6
6	Used	300	15%CO_2/He	34.8
7	Used	275	15%CO_2/He	35.1
8	Used	300	28.5%CO_2/5%H_2O/He	37.9

Figure 5 of the main paper presents the impact of the space velocity on the CO_2 capture efficiency of the $MgCa_{0.05}A_{0.20}$ material, while **Figure S3** displays the effect on the CO_2 capture rate. A decrease in material loading, or otherwise stated, an increase in space velocity results in shorter contact time between the gas and solid compounds, leading to a decline of the CO_2 capture efficiency. However, as mentioned in the main paper, this decrease is not proportional to the reduction in material loading. This infers that the decrease of the CO_2 concentration along the axial direction of the bed significantly

limits the kinetic driving force of the reaction. The smaller amount of material in the bed attains higher CO_2 capture rate compared to the higher amount of material when both are exposed to the same volumetric gas flow, with the experiment with GHSV of 2400 h^{-1} reaching a capture rate of ~0.25 mmol/min/g. However, the faster carbonation rate observed at higher GHSVs leads to a faster transition to the slower kinetically controlled stage of the CO_2 diffusion through the formed carbonate products, along with a more pronounced decrease of the performance over time in the 3rd regime.
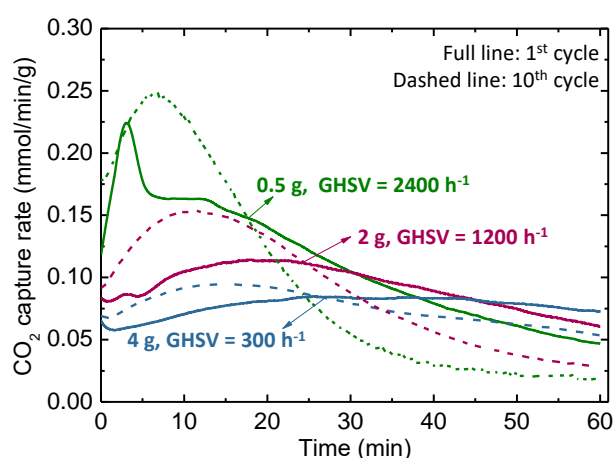
Figure S3. *CO_2 capture rate during the carbonation stage of the 1st and 10th cycle for the MgCa$_{0.05}$A$_{0.20}$ material when investigated via carbonate looping experiments in a fixed bed reactor with different space velocities for the carbonation stage (carbonation stage: 30% CO_2/He, 300°C; decarbonation stage: 450°C, 100% He, 720 h^{-1})*

References

1   T. Papalas, I. Polychronidis, A. N. Antzaras and A. A. Lemonidou, *J CO2 Util*, 2021, **50**, 101605.

2   J. Chen, L. Duan, F. Donat and C. R. Müller, *ACS Sustain Chem Eng*, 2021, **9**, 6659–6672.

3   H. Cui, Q. Zhang, Y. Hu, C. Peng, X. Fang, Z. Cheng, V. V. Galvita and Z. Zhou, *ACS Appl Mater Inter*, 2018, **10**, 20611–20620.

4   J. J. Arcenegui Troya, V. Moreno, P. E. Sanchez-Jiménez, A. Perejón, J. M. Valverde and L. A. Pérez-Maqueda, *ACS Sustain Chem Eng*, 2022, **10**, 850–859.